WAVELENGTH DOES NOT EQUAL PRESSURE: VERTICAL CONTRIBUTION FUNCTIONS AND THEIR IMPLICATIONS FOR MAPPING HOT JUPITERS

IAN DOBBS-DIXON¹ AND NICOLAS B. COWAN²

ABSTRACT

Multi-band phase variations in principle allow us to infer the longitudinal temperature distributions of planets as a function of height in their atmospheres. For example, 3.6 μ m emission originates from deeper layers of the atmosphere than 4.5 μ m due to greater water vapor absorption at the longer wavelength. Since heat transport efficiency increases with pressure, we expect thermal phase curves at 3.6 μ m to exhibit smaller amplitudes and greater phase offsets than at 4.5 μ m —this trend is not observed. Of the seven hot Jupiters with full-orbit phase curves at 3.6 and 4.5 μ m, all have greater phase amplitude at 3.6 μ m than at 4.5 μ m, while four of seven exhibit a greater phase offset at 3.6 μ m. We use a 3D radiative-hydrodynamic model to calculate theoretical phase curves of HD 189733b, assuming thermo-chemical equilibrium. The model exhibits temperature, pressure, and wavelength dependent opacity, primarily driven by carbon chemistry: CO is energetically favored on the dayside, while CH₄ is favored on the cooler nightside. Infrared opacity therefore changes by orders of magnitude between day and night, producing dramatic vertical shifts in the wavelength-specific photospheres, which would complicate eclipse or phase mapping with spectral data. The model predicts greater relative phase amplitude and greater phase offset at 3.6 μ m than at 4.5 μ m, in agreement with the data. Our model qualitatively explains the observed phase curves, but is in tension with current thermo-chemical kinetics models that predict zonally uniform atmospheric composition due to transport of CO from the hot regions of the atmosphere.

¹Department of Physics, NYU Abu Dhabi PO Box 129188 Abu Dhabi, UAE

² Department of Physics and Department of Earth & Planetary Sciences, McGill University, 3550 rue University, Montréal, QC H3A 2A7, Canada

1. INTRODUCTION

If a planet has a sufficiently large day-night temperature contrast, then it will exhibit thermal phase variations: it will appear brighter in the infrared when we see its dayside than its nightside. In practice, this condition holds for short-period planets because tidal forces tend to make them rotate synchronously, with one hemisphere always facing the host star, and the other perpetually in the dark (e.g., Dobbs-Dixon et al. 2004). Regardless of their underlying rotational state, thermal phase measurements indicate that short period planets have day-night temperature contrasts of hundreds to thousands of Kelvin (Cowan & Agol 2011a; Perez-Becker & Showman 2013; Schwartz & Cowan 2015; Komacek & Showman 2016; Schwartz et al. 2017).

As a consequence of day-to-night heat transport, the hottest point on the planet may be displaced from the permanent sub-stellar location. This symmetry breaking occurs because even a tidally locked planet rotates in an inertial frame. The resulting coriolis forces couple to the day-night temperature differential to accelerate a super-rotating circumplanetary jet (Showman & Polvani 2011; Tsai et al. 2014). Atmospheric circulation models of tidally locked hot Jupiters almost uniformly predict the atmosphere to be dominated by a broad superrotating equatorial jet (e.g., Heng & Showman 2014, and references therein). This leads to the general prediction that their thermal phase variations will peak prior to superior conjunction, when regions east of the substellar longitude are facing the observer (east is defined to be in the direction of the planet's rotation). This phase offset has indeed been observed for many hot Jupiters, starting with HD 189733b (Knutson et al. 2007, 2009, 2012).

Given the successes of eclipse and phase mapping using Spitzer, Kepler, and Hubble, it is now expected that the James Webb Space Telescope will enable 3D mapping of the daysides of hot Jupiters and 2D longitude-pressure maps of their nightsides (for a review of exoplanet mapping, see Cowan & Fujii 2017). Different wavelengths have different opacities and hence probe different pressures in the atmosphere: the optical depth to the top-of-atmosphere is proportional to the mass of overlying gas, as is the pressure, so optical depth and pressure should be intimately linked, provided that the opacity spectrum is roughly constant throughout the entire atmosphere.

In Section 2 we discuss current trends in *Spitzer* phase curves of hot Jupiters, including two trends that seem to defy expectations. In Section 3 we use a radiative-hydrodynamic model to explore the longitudinal dependence of vertical contribution functions for HD 189733b

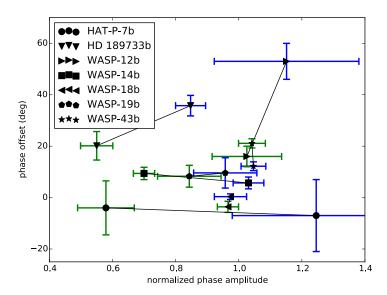


Figure 1. Phase offset versus normalized phase amplitude for six hot Jupiters. The normalized phase amplitude is given by $(F_{\rm max}-F_{\rm min})/F_{\rm day}$. Blue denotes 3.6 μ m, while green is 4.5 μ m; each planet is denoted by different symbols and the two wavebands for a given planet are connected by a line to guide the eye. The most robust trend is that the normalized phase amplitude is always greater at 3.6 μ m than at 4.5 μ m (blue points are always to the right of green points). In addition, HD 189733b, WASP-12b, WASP-18b, and WASP-19b exhibit greater phase offsets at the wavelength with the greatest normalized amplitude. Neither of these trends is expected. Naively we would expect the blue points to be found to the upper left of the green points.

and find that we can qualitatively explain the trends in Spitzer phase curves. We discuss our findings and their implications in Section 4

2. TRENDS IN THE *SPITZER* PHASE MEASUREMENTS OF HOT JUPITERS

Thermal phase measurements have been made with the Spitzer Space Telescope (Werner et al. 2004) for a dozen planets. For consistency, we only consider full-orbit, continuous phase measurements of planets on circular orbits acquired with both the 3.6 and 4.5 μ m channels of the Infrared Array Camera (IRAC; Fazio et al. 2004). Our sample therefore consists of seven planets: WASP-12b (Cowan et al. 2012a), HD 189733b (Knutson et al. 2012), WASP-18b (Maxted et al. 2013), WASP-14b (Wong et al. 2015), HAT-P-7b and WASP-19b (Wong et al. 2016), and WASP-43b (Stevenson et al. 2017).

In Figure 1 we plot the phase offset (the angular separation between the peak of the phase curve and superior conjunction) vs. the normalized phase amplitude (the peak-to-trough amplitude of phase variations divided by the eclipse depth at that wavelength). To first

order, the phase offset is equal to the longitudinal distance between the sub-stellar point and the zonally offset hotspot, but they are not interchangeable (Cowan & Agol 2008; Schwartz et al. 2017), while the normalized amplitude is related to the day–night brightness contrast (see further discussion in Section 3). These data show two trends: (1) the normalized amplitude of phase variations is always greater at 3.6 μ m than at 4.5 μ m, and (2) the phase offset is usually greater at 3.6 μ m than at 4.5 μ m. Note that the second trend is not nearly as statistically significant as the first.

One-dimensional clear-sky thermo-chemical equilibrium models of HD 189733b predict that 3.6 μ m photons originate from deeper in the atmosphere than 4.5 μ m photons on both the dayside and nightside (Figure 8 of Knutson et al. 2009). Since radiative timescales increase with depth, we would expect smaller amplitude phase variations at 3.6 μ m than at 4.5 μ m—assuming similar advective timescales (wind speeds) at all pressures. This naïve prediction is clearly ruled out by the data shown in Figure 1.

Moreover, intuition of damped driven oscillators (and energy balance models: Cowan & Agol 2011b; Zhang & Showman 2017) suggests that phase offset and normalized amplitude should be anti-correlated, with large amplitude phase variations necessarily having a small phase offset (e.g., Appendix A of Schwartz et al. 2017). This trend is also not seen: four of the seven planets (HD 189733b, WASP-12b, WASP-18b, and WASP-19b) instead exhibit greater phase offsets at the wavelength with the greatest normalized amplitude. Though the equilibrium temperatures and surface gravities of these planets vary, simulations (see Heng & Showman 2014) of a wide array of planets exhibit a dynamical structure comparable to HD 189733b, so we expect similar behavior.

3. PREDICTIONS FROM A RADIATIVE-HYDRODYNAMIC MODEL OF HD 189733b

To explore these phenomena, we use a radiative hydrodynamic code that solves the fully compressible Navier-Stokes equations coupled with wavelength-dependent radiative transfer to simulate the planetary atmosphere of HD 189733b (Dobbs-Dixon & Agol 2013). The equations are solved in spherical coordinates with resolution $\{N_r, N_\phi, N_\theta\} = \{100, 160, 64\}$, where r is the radial distance, ϕ is the longitude, and θ is the latitude. Transfer of energy via radiation employs a frequency-dependent two-stream approximation (Mihalas 1978). The full planetary spectrum is divided in 30 bins utilizing averaged frequency-dependent opacities from Sharp

& Burrows (2007). A broad super-rotating equatorial jet and counter rotating mid latitude jets are the dominant dynamical features, similar to many others in the literature. Observable quantities are calculated by tracing rays through the simulated atmosphere at 5000 wavelengths between 0.3 and 30 μ m. Qualitatively, the model is seen to match transit, eclipse, and phase curve observations, though quantitative differences remain (see below). Further, though we present simulations only of HD 189733b, as discussed above, the underlying dynamical features exhibited in this atmosphere are expected to be applicable to a wide range of planets. More on both the radiative-hydrodynamic simulation and the method of calculating observable quantities can be found in Dobbs-Dixon & Agol (2013).

To compare our simulation to Figure 1 we calculate both the phase offset and the normalized phase amplitude. This is done by first calculating a theoretical phase curve from the model; essentially a compilation of emission spectra as the sub-observer longitude moves around the planet as it would throughout an orbit. Once we have a wavelength dependent phase curve, we bin it using the IRAC and MIPS band-passes to assemble the phase curves for any bandpass. From these band averaged phase curves, it is trivial to fit for maximum flux, minimum flux, and the offset of the maximum flux. The results are plotted in Figure 2. Small colored dots represent a subset of individual wavelengths, while the bandintegrated quantities are denoted by large colored dots. The predicted 3.6 μ m phase curve has a greater amplitude and phase offset than the 4.5 μ m phase curve, as observed for HD 189733b and many other hot Jupiters (cf. Figures 1 and 2). However, though we match the relative locations of the 3.6 and 4.5 μ m bands, they do not match quantitatively. This was recognized in Dobbs-Dixon & Agol (2013), who noted that the phase offsets in the model were uniformly under-predicted, suggesting the need for either a stronger jet or a longer radiative timescale. In fact, no current 3D models quantitatively predict the phase offset, with most other models overpredicting it (e.g. Showman et al. 2009).

Though we have presented phase amplitudes in terms of flux, one must be a bit cautious. If the day and night sides of the planet were isothermal, with hotter and cooler temperatures respectively, the nature of the blackbody emission would naturally produce a larger phase amplitude at 3.6 μ m then 4.5 μ m. One potential solution is to explore the brightness temperature as a function of phase instead. In Figure 3 we show T_{bright} as a function of wavelength for several representative phases. The strongly non-isothermal nature of the atmosphere in the radial direction leads to large

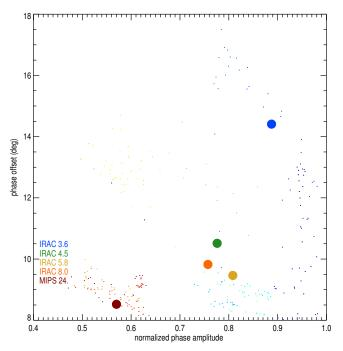


Figure 2. Phase offset vs. normalized phase amplitude from the radiative-hydrodynamical model of HD 189733b. The normalized phase amplitude is given by $(F_{\text{max}} - F_{\text{min}})/F_{\text{day}}$. Small dots illustrate values at a subset of the individual wavelengths (colored from red to blue with decreasing wavelength), while the larger dots are the IRAC and MIPS bandaveraged quantities. Both quantities are extracted from wavelength dependent theoretical phase curves generated by ray tracing through the radiative-hydrodynamical model. As the phase curves are not sinusoidal, we utilize the simulated fluxes at phases near the maximum and minimum to fit for F_{max} , the offset, and F_{min} . F_{day} is the planetary flux during eclipse. Consistent with the observations presented in Figure 1, both the offset and normalized amplitude at 3.6 μ m are greater than at 4.5 μ m. Offsets at 5.8 μ m, 8.0 μ m, and 24.0 μ m are smaller and quite similar as they are probing the upper regions of the atmosphere (see text). The varying phase amplitude for these bands comes from the convoluted structure of their contribution functions with longitude, shown in Figure 4.

wavelength dependence in addition to the expected longitudinal dependence. For this reason, coupled to the fact that brightness temperature is a more derived quantity leading to larger uncertainties, we choose to present fluxes. Never the less, as can be read off the IRAC bandaveraged points in the figure, the differential in brightness temperature between day and night is also larger at 3.6 μ m than at 4.5 μ m. This trend is similarly born out in the observations of HD 189733b.

In an attempt to elucidate the mechanism behind the unintuitive results of Figures 1, 2, and 3, we calculate the longitudinally dependent vertical contribution function at the equator from our model. The contribution

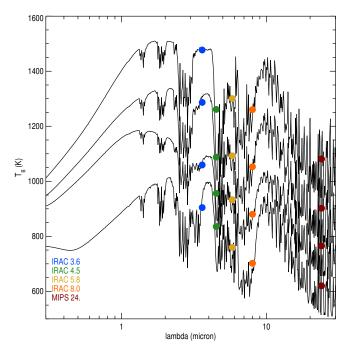


Figure 3. Brightness temperatures as a function of wavelength calculated from the results of the radiative hydrodynamics simulation for several representative orbital phases. Increasing from the bottom, the curves represent observations looking at the anti-stellar point, the western terminator, the eastern terminator, and the substellar point. Colored dots denote the IRAC and MIPS band averaged brightness temperature. The strongly non-isothermal nature of the atmosphere at each phase, coupled to the strongly wavelength dependent opacity and associated contribution function (see text and Figure 4) lead to widely varying temperatures.

function is given by (Chamberlain & Hunten 1987):

$$cf(P,\lambda) = B(\lambda,T) \frac{de^{\tau}}{d\log P},$$
 (1)

where τ is the wavelength dependent optical depth and B is the local blackbody. The results are shown in Figure 4. On the left-hand side, the gray scale shows the temperature as a function of pressure and longitude along the equator, with the sub-stellar point located at zero degrees longitude. Colored bands indicate the regions of the atmospheres near the peak of the contribution functions. The complicated pressure-longitude structure of the contribution functions is immediately obvious. For example, the 3.6 μ m photosphere lies at —or above— the 4.5 μ m photosphere on the planet's dayside. On the nightside, on the other hand, the usual adage "ch1 probes deeper" is actually borne out.

The convoluted contribution functions arise due to the temperature, pressure, and wavelength dependence of opacity, which can increase in one band while simultaneously decreasing in another. The result is that the effective photospheres in the various bands can cross, imply-

ing that we are probing different respective depths and pressures in the atmosphere at different orbital phases. The right-hand panel of Figure 4 shows the vertical contribution functions at the substellar and antistellar points. From these plots it is clear that the contribution functions are far from delta-functions, but in fact probe large ranges in pressures and can exhibit several maxima.

There are a number of features in Figure 4 that manifest themselves in Figure 2. Starting with the 5.8, 8.0, and 24 μ m bands, we see that they probe low pressure regions on the dayside. Given the short radiative timescales at these low pressures, the hot-spot displacement is quite low resulting in small phase offsets. The rather low phase offset of the 4.5 μ m point is the result of two features: the curved nature of the photosphere and the multiple peaks of the contribution function with height as seen in the right-hand panel. The curvature of the photosphere means it is probing cooler temperatures as it moves away from the sub-stellar point, making the dayside brightness map of the planet more centrally concentrated (essentially like limb-darkening). The second effect, the double peaked contribution function, means that a significant fraction of the emission is coming from higher in the atmosphere, where again the short radiative timescale tends to reduce the phase offset. The 3.6 μ m photosphere, on the other hand, is roughly an isobar on the dayside, hence the greater phase offset at $3.6 \ \mu m.$

Phase amplitudes can also be essentially read off Figure 4. The peak of the contribution function for the 24 μ m band remains high in the atmosphere, where it is cool across the entire planet, resulting in the smallest phase amplitude. The phase amplitudes at 5.8 and 8.0 μ m are similar, though the 5.8 μ m crosses more temperature contours, resulting a slightly larger value. At first glance, the relative phase amplitudes at 4.5 and 3.6 μ m seem to defy the others. However, as can again be seen in the right-hand panel, the significant contribution at 4.5 μ m from the upper, cooler regions of the atmosphere produce a lower value of $F_{\rm max}$ relative to 3.6 μ m and lead to a smaller phase amplitude.

The convoluted photospheres are due to changes in opacity with temperature and pressure. The radiative-hydrodynamical models utilize opacities from Sharp & Burrows (2007), which assume solar abundance and thermo-chemical equilibrium at each temperature and pressure (i.e.: location) in the atmosphere. The opacities include absorption due to the four most spectroscopically active species, H₂O, CO, CO₂, and CH₄. The assumption of thermo-chemical equilibrium is important, and we discuss below.

To understand the behavior of opacity in the current simulations, we plot the opacity structure with temperature and pressure at four representative wavelengths in Figure 5. Note that these are opacities at single wavelengths at the center of the IRAC bands, not band averaged quantities. The most obvious feature in the plots is the transition running diagonally in all 4 of the plots, which corresponds to the CO-CH₄ transition. The pressures and temperatures of HD 189733b happen to straddle this boundary. By following an isobar across each of the plots one can get a rough idea of the opacity as a function of longitude near the contribution function maximum. Of particular note, the opacity at 3.6 μ m increases by orders of magnitude when moving from day to night, while at 4.5 μ m it decreases. The fact that they are not correlated leads directly to the crossing of contribution functions with longitude—a given wavelength cannot be assumed to always probe deeper/shallower than another. Though the carbon chemistry likely plays an important role in explaining the trend for HD 189733b, planets with hotter or cooler atmospheres may not straddle this transition. None the less, as seen in Figure 1 planets with a wide range of parameters exhibit this counterintuitive result. As we discuss below, additional physics, including vertical mixing and inhomogeneous clouds may result in similar phenomena.

4. DISCUSSION & CONCLUSIONS

4.1. Clouds & Disequilibrium Chemistry

We've used a cloud-free Solar-abundance model where the atmosphere is everywhere in thermo-chemical equilibrium. Clouds could in principle change this story in two ways. First of all, condensation can reduce gas phase abundances by orders of magnitude. But the dominant absorbers in the Spitzer IRAC channels, H₂O, CO, CO₂, and CH₄, do not condense anywhere in the atmosphere of a hot Jupiter. More importantly, mineral condensates increase the opacity, and do so in a relatively gray fashion. Uniform clouds would therefore lead to contribution functions that are less wavelengthdependent. Inhomogeneous clouds, as have been inferred based on optical phase curves (Demory et al. 2013; Esteves et al. 2015; Angerhausen et al. 2015) and simulations (Lee et al. 2016), would complicate the picture, with cloudy regions having overlapping contribution functions and clear regions exhibiting the temperaturedependent effects we've discussed in this paper.

Knutson et al. (2012) suggested that the nightside of HD 189733b might not be in thermo-chemical equilibrium. The observed nightside brightness temperature is greater at 4.5 than at 3.6 μ m, which could be ex-

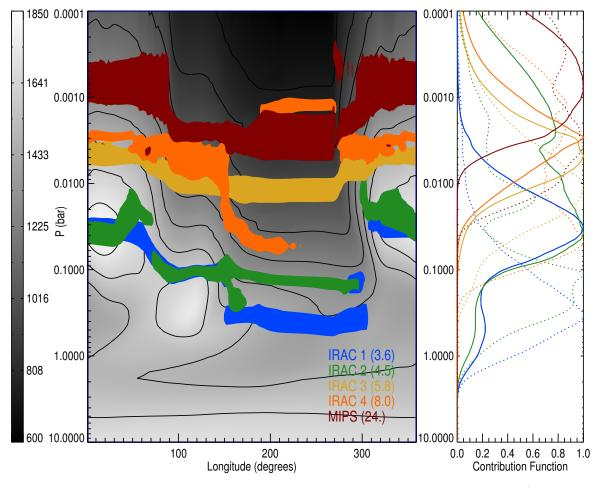


Figure 4. Left: The peaks of the normalized contribution functions for the IRAC and MIPS bands (colored bands) overplotted on the temperature in K (gray scale) as a function of pressure and longitude in degrees along the equator. The sub-stellar longitude is at zero. Right: The vertical contribution functions at the sub-stellar (solid) and anti-stellar (dotted) locations. The complex vertical temperature-pressure structure, shaped by the underlying radiative hydrodynamics in the model, is clearly a strong function of longitude. Assuming thermo-chemical equilibrium, this leads to significant variations in the opacities of individual bands, in a manner that does not necessary correlate. The result is that the radial location of the effective photospheres in the bands do not necessarily maintain their relative positions as you move around in longitude.

plained if CO from deeper layers, or the dayside, were transported to the vicinity of the IR photosphere faster than the chemical timescale (Madhusudhan et al. 2016). Indeed, Cooper & Showman (2006) predicted that atmospheric dynamics could mix hot Jupiter atmospheres faster than chemistry can operate. Agúndez et al. (2014) predicted that HD 189733b should have CO rather than $\mathrm{CH_4}$ everywhere in the atmosphere due to horizontal quenching.

Stevenson et al. (2010) reported disequilibrium chemistry on GJ 436b based on its dayside emission spectrum: they saw evidence for CO rather than $\mathrm{CH_4}$. Since even the substellar photospheric temperature is too cool for CO, the gas must originate from deeper layers of the atmosphere, so-called vertical quenching. Vertical mixing on HD 189733b could also increase the CO abundance at the nightside photosphere, since at pressures of ~ 1 bar,

CO is preferred everywhere. Interestingly, at pressures above ~ 10 bar, CH₄ again becomes the dominant species (e.g., Figure 2 of Madhusudhan et al. 2016), so vertical mixing cuts both ways.

If hot Jupiter atmospheres are well mixed, then the temperature-dependent effects we discuss in this Letter are less dramatic, but still important. In particular, the curious shape of the 4.5 μ m photosphere — which partially explains the small phase offsets at this wavelength— is not driven by carbon chemistry.

In any case, HD 189733b is the coolest and most longitudinally isothermal hot Jupiter that has been studied to date (Schwartz & Cowan 2015; Schwartz et al. 2017). Most hot Jupiters with published phase curves have much greater longitudinal temperature contrasts, often measured in thousands, rather than hundreds, of K. And the very hottest of them have dayside temper-

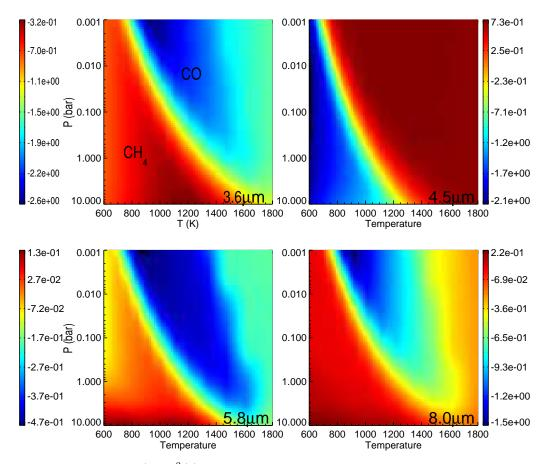


Figure 5. The log of the total opacity (in cm²/g) due to molecules as a function of temperature and pressure at 3.6 μ m, 4.5 μ m, 5.8 μ m, and 8.0 μ m. The opacities are taken from Sharp & Burrows (2007) and assume thermo-chemical equilibrium at each temperature and pressure. The obvious feature running diagonally through all the plots is the change in opacity as the dominate carbon-bearing molecule switches from CH₄ in the lower left to CO in the upper right. At a given pressure, the increase of the opacity at 4.5 μ m with temperature (as opposed to the decrease at the other three wavelengths) plays an important role in dictating the relative radial location of the photospheres with longitude. Note these are not band averaged quantities, but instead focus just on the central wavelength of the band.

atures hot enough to dissociate molecules and ionize atoms, e.g. WASP-12b (Hebb et al. 2009), WASP-33b (Smith et al. 2011), and KELT-9b (Gaudi et al. 2017). These transitions should lead to enormous opacity differences between night and day and hence large excursions in the wavelength-specific contribution functions. It is not clear to what extent horizontal and vertical mixing can homogenize the atmospheres of such worlds.

4.2. Implications of Non-Isobaric Photospheres

The wavelength-dependent photospheres are not the concentric spheres we like to imagine. This does not necessarily impact estimates of effective temperatures: many schemes to go from brightness temperatures to an effective temperature are agnostic about the precise pressures probed by different wavelengths (Cowan & Agol 2011a; Schwartz & Cowan 2015), though energy budgets based on spectral retrieval may be more sensitive (e.g., Stevenson et al. 2014). Nor do non-

isobaric photospheres invalidate eclipse and phase mapping, either in a single broadband, in multiple bands, or even spectral mapping (limb-darkening could in principle scuttle thermal mapping efforts, but it has previously been shown to be negligible: Cowan & Agol 2008).

However, convoluted photospheres do complicate the interpretation of multi-wavelength maps. In particular, we have shown that automatically assuming that different wavelengths probe different layers is incorrect: it is approximately true at any one longitude and latitude on a planet, but the locations and order of the layers change from one location to another, primarily driven by differences in temperature coupled with a temperature-dependent opacity spectrum.

In order to construct multi-dimensional maps of hot Jupiters, we will have to do something more clever than constructing a layer-cake of multiple single-wavelength maps. One could instead start by evaluating the vertical temperature profile at each location on the maps —especially the regions near the equator that contribute most to the lightcurves and hence are best-constrained (this step is not the same as performing spectral retrieval on disk-integrated spectra as was done by Stevenson et al. 2014). One would then combine these vertical temperature soundings to construct a true 3D map of the planet's temperature structure (with the usual caveat that the latitudinal constraints on the nightside are weak and indirect: Majeau et al. 2012; de Wit et al. 2012; Cowan et al. 2013). The challenge with this approach will be assessing the uncertainty in the brightness maps at each location in a way that is useful for spectral retrieval exercises.

Alternatively, it may be possible to fit the disk-integrated multi-wavelength data simultaneously with a model that accounts not only for 3D variations in temperature, but also for the wandering photospheres. In any case, this is a problem worth tackling soon given the impending launch of the James Webb Space Telescope.

We thank the International Space Science Institute for hosting the Exo-Cartography workshops. N.B.C. acknowledges support from the McGill Space Institute, l'Institut de recherche sur les exoplanètes, an NSERC Discovery grant, and a FRQNT Nouveau Chercheur grant. The authors further thank the anonymous referee for improvements to the paper.

REFERENCES

- Agúndez, M., Parmentier, V., Venot, O., Hersant, F., & Selsis, F. 2014, A&A, 564, A73
- Angerhausen, D., DeLarme, E., & Morse, J. A. 2015, Publications of the Astronomical Society of the Pacific, 127, 1113
- Chamberlain, J. W., & Hunten, D. M. 1987, Theory of planetary atmospheres. An introduction to their physics and chemistry (Academic Press)
- Cooper, C. S., & Showman, A. P. 2006, ApJ, 649, 1048
- Cowan, N. B., & Agol, E. 2008, ApJL, 678, L129
- Cowan, N. B., & Agol, E. 2011a, The Astrophysical Journal, 729, 54
- —. 2011b, The Astrophysical Journal, 726, 82
- Cowan, N. B., Fuentes, P. A., & Haggard, H. M. 2013, Monthly Notices of the Royal Astronomical Society, 434, 2465
- Cowan, N. B., & Fujii, Y. 2017, ArXiv e-prints, arXiv:1704.07832
- Cowan, N. B., Machalek, P., Croll, B., et al. 2012a, The Astrophysical Journal, 747, 82
- Cowan, N. B., Voigt, A., & Abbot, D. S. 2012b, The Astrophysical Journal, 757, 80
- de Wit, J., Gillon, M., Demory, B.-O., & Seager, S. 2012, A&A, 548, A128
- Demory, B.-O., De Wit, J., Lewis, N., et al. 2013, The Astrophysical Journal Letters, 776, L25
- Dobbs-Dixon, I., & Agol, E. 2013, MNRAS, 435, 3159
- Dobbs-Dixon, I., Lin, D. N. C., & Mardling, R. A. 2004, ApJ, 610, 464
- Esteves, L. J., De Mooij, E. J., & Jayawardhana, R. 2015, The Astrophysical Journal, 804, 150
- Fazio, G. G., Hora, J. L., Allen, L. E., et al. 2004, ApJS, 154, 10

- Gaudi, B. S., Stassun, K. G., Collins, K. A., et al. 2017, Nature, 546, 514
- Hebb, L., Collier-Cameron, A., Loeillet, B., et al. 2009, The Astrophysical Journal, 693, 1920
- Heng, K., & Showman, A. P. 2014, arXiv preprint arXiv:1407.4150
- Knutson, H. A., Charbonneau, D., Allen, L. E., et al. 2007, Nature, 447, 183
- Knutson, H. A., Charbonneau, D., Cowan, N. B., et al. 2009, The Astrophysical Journal, 690, 822
- Knutson, H. A., Lewis, N., Fortney, J. J., et al. 2012, The Astrophysical Journal, 754, 22
- Komacek, T. D., & Showman, A. P. 2016, The Astrophysical Journal, 821, 16
- Lee, G., Dobbs-Dixon, I., Helling, C., Bognar, K., & Woitke, P. 2016, A&A, 594, A48
- Madhusudhan, N., Agúndez, M., Moses, J. I., & Hu, Y. 2016, SSRv, 205, 285
- Majeau, C., Agol, E., & Cowan, N. B. 2012, ApJL, 747, L20
- Maxted, P., Anderson, D., Doyle, A., et al. 2013, Monthly Notices of the Royal Astronomical Society, 428, 2645
- Mihalas, D. 1978, Stellar atmospheres /2nd edition/
- Perez-Becker, D., & Showman, A. P. 2013, The Astrophysical Journal, 776, 134
- Schwartz, J. C., & Cowan, N. B. 2015, Monthly Notices of the Royal Astronomical Society, 449, 4192
- Schwartz, J. C., Kashner, Z., Jovmir, D., & Cowan, N. B. 2017, ArXiv e-prints, arXiv:1707.05790
- Sharp, C. M., & Burrows, A. 2007, ApJS, 168, 140
- Showman, A. P., Fortney, J. J., Lian, Y., et al. 2009, The Astrophysical Journal, 699, 564
- Showman, A. P., & Polvani, L. M. 2011, ApJ, 738, 71

- Smith, A. M. S., Anderson, D. R., Skillen, I., Collier Cameron, A., & Smalley, B. 2011, MNRAS, 416, 2096
- Stevenson, K. B., Harrington, J., Nymeyer, S., et al. 2010, Nature, 464, 1161
- Stevenson, K. B., Désert, J.-M., Line, M. R., et al. 2014, Science, 346, 838. http://www.sciencemag.org/ content/346/6211/838.abstract
- Stevenson, K. B., Line, M. R., Bean, J. L., et al. 2017, The Astronomical Journal, 153, 68

- Tsai, S.-M., Dobbs-Dixon, I., & Gu, P.-G. 2014, ApJ, 793, 141
- Werner, M. W., Roellig, T. L., Low, F. J., et al. 2004, ApJS, 154, 1
- Wong, I., Knutson, H. A., Lewis, N. K., et al. 2015, The Astrophysical Journal, 811, 122
- Wong, I., Knutson, H. A., Kataria, T., et al. 2016, The Astrophysical Journal, 823, 122
- Zhang, X., & Showman, A. P. 2017, The Astrophysical Journal, 836, 73